Korean Journal of Remote Sensing, Vol.22, No.1, 2006, pp.25~40

A Statistical Analysis of JERS L-band SAR Backscatter and Coherence Data for Forest Type Discrimination

Cheng Zhu and Soojeong Myeong †

Program in Environmental and Resource Engineering
SUNY College of Environmental Science and Forestry, Syracuse, NY 13210, USA

Abstract : Synthetic aperture radar (SAR) from satellites provides the opportunity to regularly incorporate microwave information into forest classification. Radar backscatter can improve classification accuracy, and SAR interferometry could provide improved thematic information through the use of coherence. This research examined the potential of using multi-temporal JERS-1 SAR (L band) backscatter information and interferometry in distinguishing forest classes of mountainous areas in the Northeastern U.S. for future forest mapping and monitoring.

Raw image data from a pair of images were processed to produce coherence and backscatter data. To improve the geometric characteristics of both the coherence and the backscatter images, this study used the interferometric techniques. It was necessary to radiometrically correct radar backscatter to account for the effect of topography. This study developed a simplified method of radiometric correction for SAR imagery over the hilly terrain, and compared the forest-type discriminatory powers of the radar backscatter, the multi-temporal backscatter, the coherence, and the backscatter combined with the coherence. Statistical analysis showed that the method of radiometric correction has a substantial potential in separating forest types, and the coherence produced from an interferometric pair of images also showed a potential for distinguishing forest classes even though heavily forested conditions and long time separation of the images had limitations in the ability to get a high quality coherence. The method of combining the backscatter images from two different dates and the coherence in a multivariate approach in identifying forest types showed some potential. However, multi-temporal analysis of the backscatter was inconclusive because leaves were not the primary scatterers of a forest canopy at the L-band wavelengths. Further research in forest classification is suggested using diverse band width SAR imagery and fusing with other imagery source.

Key Words : JERS-1, L-band SAR, backscatter, coherence, forest classification.

1. Introduction

Accurate and detailed information about forest types and their spatial distribution is fundamental to forest management. In the Northeastern U. S. A., forests are often complex mixtures of diverse species

Received 15 September 2005; Accepted 6 February 2006.
† Corresponding Author: S. Myeong (smyeong@syr.edu)

and structures. The same species might occur in different forest type classes and in different proportions or associations. Forested areas might be mixtures of deciduous and coniferous species. Following the convention in this academic field, the first will be called the hardwood in this paper, and second, the softwood. Previous research revealed that optical satellite imagery is generally insufficient for distinguishing hardwood and softwood forests from mixed forests and the separation of more specific types is usually even less successful (Singh, 1994; Szymanski, 1998, 2002). Moreover, optical sensors often fail to acquire high quality data due to clouds or low light conditions, especially in the northeastern U.S. Synthetic Aperture Radar (SAR) is an active microwave sensor that is robust against weather conditions and unaffected by day or night. SAR showed some promise for providing additional and unique information for distinguishing forest types (Rignot *et al.*, 1994; Stofan *et al.*, 1995).

SAR image backscatter data consist of two components: the magnitude and the phase that are stored as complex numbers in two layers (Huurneman *et al.*, 1996). Traditionally, only the backscatter magnitude (hereafter simply called backscatter) was interpreted for the land cover classification application. Backscatter provides information on the structure and moisture condition that is complementary to the information provided by optical remote sensing. Different bandwidth and polarization combinations might provide different information of land cover. However, due to the image noise caused by coherent effects (speckle), overlapping of the backscatter patterns of the various land categories, and the strong effect of the local topography, some research indicates difficulty in deriving classes that are more detailed than simply forest when using only backscatter data with the limited bands and polarizations of current civilian satellite systems (EUFORA, 1998; Torma and Koskinen., 1997; Wegmuller and Charles, 1995).

The phase information of SAR image is mainly used in the field of interferometry which is a technique for extracting three dimensional information of the Earth's surface (Gens and Van Genderen, 1996). Repeat pass interferometry is the most common technique used to acquire interferometric data by spaceborne SAR sensors. The satellite passes in nearly the same orbit to cover an area twice with a slightly different viewing angle. The phase information can then be used to measure the differences in path length between the target and the two sensor positions. The main output of interferometry of SAR data is topographic information about the terrain heights or the monitoring of positional changes of the Earth surface. A strong relationship exists between the quality of these products and the correlation of the complex data sets, which is characterized by the "interferometric correlation" (Huurneman *et al.*, 1996). Interferometric correlation is a measure of the variance of the interferometric phase estimates. The interferometric correlation coefficient (which is called degree of coherence) decreases with increasing volume scattering and temporal changes. Therefore, coherence contains thematic information that is useful for land cover and forest mapping (Askne *et al.*, 1997; Wegmuller and Werner, 1995; Wegmuller *et al.*, 1997).

Recently, a number of satellite radar remote sensing systems started to provide SAR data to the civilian community in a variety of microwave wavelengths on a routine basis. Specifically, JERS-1, which has stopped working, once provided SAR data in L-band (23cm wavelength) with HH polarization, ERS-1/2 in C-band (5.6cm) with VV polarization, and Radarsat in C-band with HH polarization. The data from these systems have shown their utility for some specific forestry applications although most applications of JERS were implemented in mapping the tropical area

rather than boreal and temperate forest (Angelis *et al.*, 2002; Rodes *et al.*, 2002; Sgrenzaroli *et al.*, 2002 ; Simard *et al.*, 2002; Salas *et al.*, 2002a, 2002b). Since the L-band SAR interacts in forests with the primary and secondary branches and trunks and sensitive to forest characteristics, it may be more useful than other imagery sources in distinguishing hardwood from softwood (Angelis *et al.*, 2002; Shimada and Isoguchi, 2002). Moreover, most interferometry studies have concentrated on classifying forest from non-forest, or retrieving forest parameters using the C-band coherence from ERS-1 3-day repeat-pass or ERS-1/2 tandem interferometric image pairs (Askne *et al.*, 1997; Huurneman *et al.*, 1996; Strozzi *et al.*, 2000; Wegmuller and Werner, 1995, 1997). Few have studied forest type classification, especially classification with JERS-1 44-day repeat-pass interferometric coherence for the boreal or temperate forest. Although the Remote Sensing Technology Center of Japan (RESTEC) stopped providing JERS imagery, it is meaningful to examine the capability of various bandwidths of SAR for future sensor development and applications. The general hypothesis of this study is that the L-band SAR data may provide enough information to better distinguish hardwood, softwood, and mixed forest. This study analyzed two JERS-1 images that are suitable for repeat pass interferometric processing in distinguishing forest types. This study focused on statistical analysis of the data from three different forest classes. The specific objectives of this study were: 1) to assess the use of only backscatter to differentiate the three forest classes examining both single date and multi-date backscatter image data; and 2) to evaluate the utility of interferometric coherence in differentiate the forest classes.

2. Methods and Materials

1) Study Area/Reference Information

The study area was the Huntington Wildlife Forest and its vicinity in the central Adirondack Mountain areas of New York State, the U. S. A. (Figure 1). The Huntington Wildlife Forest covers approximately 6,000 hectares with topography that can be characterized as rugged and mountainous. Numerous lakes of this area were created by glacial activity and elevations range from 475m to 820m above sea level. The vegetation is transitional between the boreal forests of Canada and the hardwood forests to the south. The forest stands are approximately 70% hardwood and 30% softwood and the major forest tree types are sugar maple, yellow birch, and beech.

A total of 17 softwood (estimated more than 70% softwood), 18 hardwood (estimated less than 30% softwood), and 16 mixedwood (estimated 30% to 70% softwood) sampling sites were identified through high resolution aerial photo interpretation and some supplemental field visits. These plots intended to be even more distinct with hardwood and softwood being nearly pure and the mixed being close to 50% of each. For each sample site, data

Figure 1. Huntington Wildlife Forest, the Location of the Study Area.

values including backscatter and coherence were calculated by averaging the image values in a 100m by 100m window, effectively removing the effects of speckle. The general slope of the study area was about 15 degree, and the aspects of the study area consist of four directions evenly.

This study used Digital Elevation Model (DEM) data produced by the New York State Department of Environmental Conservation in cooperation with the U. S. Geological Survey (USGS, 1998). The DEMs used Universal Transverse Mercator (UTM) Zone 18 coordinates (NAD27) and had a horizontal resolution of 10m and a vertical resolution of 0.1m. Covering the study area required a mosaic of six 7.5 minute quadrangle DEMs.

2) Imagery and software

JERS-1 L-band SAR image data was purchased directly from RESTEC in level 0 format (raw data). A repeat-pass interferometric pair was available for the study area with acquisition dates of 26 April, 1995 and 09 June, 1995. The April image was acquired during leaf-off and the June image exhibited the leaf-on condition. The interferometric baseline for this pair of images was 350m.

This study used the 1m high spatial resolution digital aerial imagery collected by the Emerge system (Kinn, 2002). This imagery assisted while generating ground reference information. This digital aerial data exhibited one-meter spatial resolution and was terrain corrected to UTM coordinates (Zone 18, NAD83). The aerial imagery of two dates was collected: April 1998 (leaf-off conditions) and October 1998 (high degree of foliage senescence). Both image collections included three spectral channels corresponding to the green, red, and near-infrared portions of the electromagnetic spectrum.

Earthview APP (Advanced Precision Processor) for SAR 1.5 (Atlantis Scientific Inc.) was used for processing the Single Look Complex (SLC) images from raw data. EVInSAR 1.2 (Atlantis Scientific Inc.) was used for calculating coherence and also for geocoding coherence and backscatter images. Supplemental software for mosaicking DEMs and choosing reference points were ENVI (Research Systems Inc.), ARC/INFO (Environmental Systems Research Institute), and ArcView 3.2 (Environmental Systems Research Institute). ERDAS Imagine 8.4 was used for radiometric correction and signature generation of reference points. SAS 8.00 was used for the statistical analyses such as analysis of variance and Mahalanobis distance.

3) Image Processing

The raw data for each radar image were processed by Earthview APP to produce single look complex (SLC) images with spatial resolution of about 10m in slant range and 6m in azimuth; spatial resolution 10m by 6m was found from the metadata of the sensor. SLC was kept since the purpose of this paper was to analyze the possibility of JERS data to discriminate different forest types. Therefore, it was better to retain as much information as possible from the raw data. Using multi-look and spatial speckle filtering would lose some information. The Earthview APP used a range/Doppler algorithm with secondary range compression to produce the SLC data (Curlander and McDonough, 1991; Elachi, 1988). Figure 2 shows a portion of the SLC image (magnitude) generated from the April data.

This SLC image pair was then processed by the EVInSAR software to produce an image showing the coherence of the interferometric pair. Coherence was calculated by Equation 1 according to the correlation coefficient definition (Atlantis Scientific Inc., 1999b; Wegmuller and Werner, 1995), and the coherence values (from 0 to 1) were linearly scaled from 0 to 255 for display and further analysis. Figure 3 shows

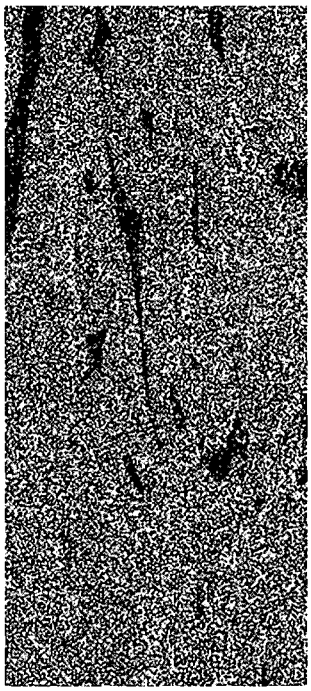

Figure 2. A Portion of the Single Look Complex Image Generated for the April Data.

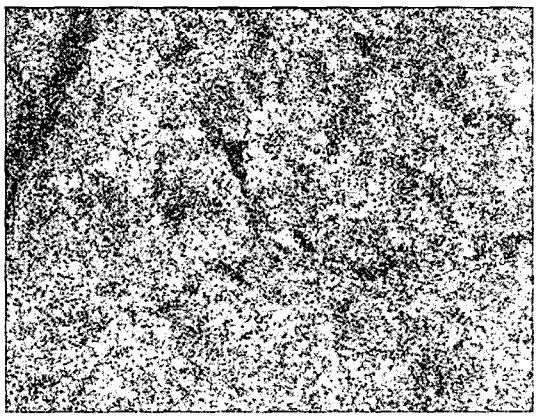

Figure 3. A Portion of the Coherence Image (not Geocoded) Generated from the April and June Data.

the coherence image that corresponds to the same area shown in Figure 2.

$$\gamma = \frac{E(g_1 g_2^*)}{\sqrt{E(g_1 g_1^*)E(g_2 g_2^*)}} \quad (1)$$

where γ is the coherence, g_1 and g_2 are the complex image values for the pair of SLC images, g_i^* means the complex conjugate of g_i, and E( ) means the expectation.

In order to relate the coherence image to the ground reference data, the coherence image had to be georectified. The normal approach to getting this georectified coherence image in EVInSAR is to complete the interferometric processing. The steps are: 1) co-register the master and slave SLC images to subpixel accuracy based on precisely predicted orbit-Earth geometry; 2) calculate the coherence and the associated interferogram; 3) apply phase unwrapping, generate a DEM in slant range; and 4) apply the geocode procedure based on this DEM. However, the coherence of our image pair was not high enough to get a good interferogram and finally could not generate a good quality DEM. Therefore, an alternative procedure in EVInSAR was used to register the SLC images with the external DEM and create a simulated external slant range DEM. EVInSAR was also used with the external DEM to estimate and remove the topography phase contributions from the InSAR pair and create a differential interferogram. After performing phase unwrapping, EVInSAR was used to add the topography back in and obtain a slant range height image (slant range DEM). This slant range DEM was then replaced by the simulated external slant range DEM and used in EVInSAR to perform the terrain correction and geocoding. The resulting coherence image was resampled to 20m pixels in the UTM coordinate system (Zone 18, NAD27). The final geocoded images (the coherence and the backscatter) were all in 20m because when registered the DEM to single look image, the Root Mean Square (RMS) error could not be less than 1 pixel since they were forested areas. Therefore, 20m was considered to be enough. Figure 4 is the geocoded coherence image. The geocoding procedure also produces geocoded single look backscatter images. Figure 5 is the

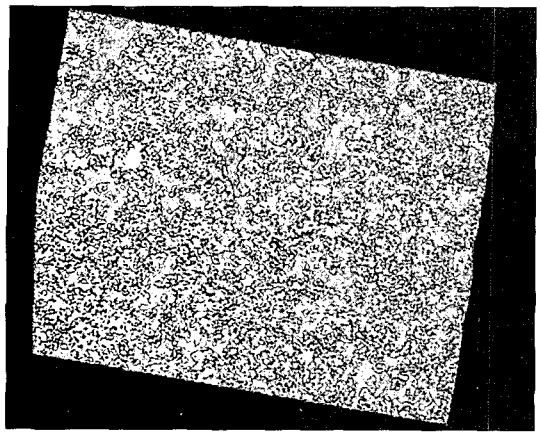

Figure 4. The Coherence Image after Geocoding.

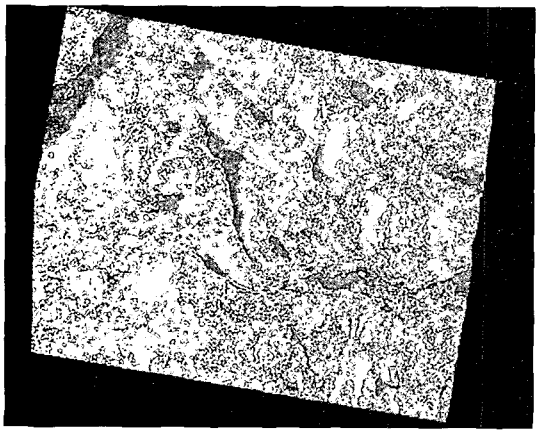

Figure 5. A Portion of the April Backscatter Image after Georectification.

georectified backscatter image from April.

To verify the results of georectification, five checkpoints in the geocoded backscatter images were compared with the same points in the orthorectified high spatial resolution Emerge aerial imagery (Kinn, 2002). The RMS error of these points in this image pair was about 15m, which was considered acceptable. Inspection of Figure 5 and statistical analysis showed that the backscatter images exhibited substantial radiometric variation over the hilly terrain due to the geometry of a side-looking sensor and the variable terrain. These variations tend to mask signal variations caused by the land cover. Therefore, radiometric correction was necessary to accomplish our research purpose.

These terrain-induced radiometric distortions are caused by the variable ground scattering area within the pixel and local incidence angle affecting the directional nature of backscatter (Van Zyl *et al.*, 1993). Therefore, radiometric corrections over the hilly terrain may be applied by normalizing the original pixel intensity by the scattering area associated with the pixel and correcting the angular variation of backscatter using empirical or theoretical models (Beaudoin *et al.*, 1995).

Conventionally, the backscatter coefficient σ° is used for forestry applications. This coefficient is defined as the average Radar Cross Section (RCS) of a patch of distributed scatterers per unit ground area (Ulaby *et al.*, 1982). The standard output product of most imaging radar is related to radar brightness β°, which is defined as the average RCS per unit image area (Raney *et al.*, 1994). Therefore, translating radar brightness to a backscatter coefficient is the first step of radiometric correction. The relation between the radar brightness and backscatter coefficient is given by the following equation (Henderson and Lewis, 1998):

$$\sigma^\circ = \sin(\alpha_{ir})\beta^\circ \qquad (2)$$

where α_{ir} is the local incidence angle in range direction, calculated by the following equation:

$$\alpha_{ir} \approx \alpha_{ref} + \theta_r = \alpha_{ref} - \arctan(\tan(\theta_n)\cos(\phi_s - \phi_n)) \qquad (3)$$

where α_{ref} is the reference incidence angle (37.5 degree for JERS-1 images in our research area), θ_r is the local ground slope in range direction, θ_n is the local ground slope, ϕ_n is the local ground aspect, and ϕ_s is the azimuth of the satellite.. The *EarthView APP User's Guide* (Atlantis Scientific Inc., 1999a) provides the following equation:

$$\beta^\circ = \frac{I^2}{\sin(\alpha_{ref})CF} \qquad (4)$$

where I is the digital number of the backscatter image, and CF is a calibration factor. CF is usually considered a constant, but is not truly constant over the images. The factor varies due to various uncompensated radiometric variations, e.g., the antenna gain, range spreading loss, propagation loss, and processor loss, which must be compensated for separately (Ulander, 1996).

The Earthview APP processor was not able to calibrate JERS-1 images, so the calibration factor of our images could not be obtained. However, from Equation (4), the digital number is proportional to the square root of radar brightness and is therefore also proportional to the square root of backscatter coefficient (Atlantis Scientific Inc., 1999; Shimada, 1996). This relation means that the digital number corrected by the scattering area I_{cor1} corresponds to the backscatter coefficient. I_{cor1} is calculated by equation 5:

$$I_{cor1} = \sqrt{\frac{\sin(\alpha_{ir})}{\sin(\alpha_{ref})}} \cdot I \qquad (5)$$

Figure 6 shows the result of this first step in the radiometric correction process as applied to the April image.

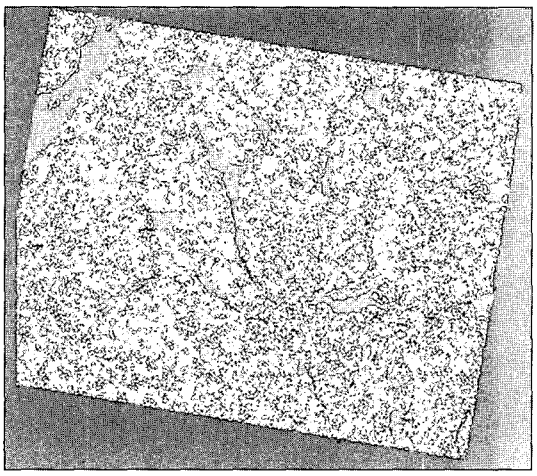

Figure 6. A Portion of the April Backscatter Image after Radiometric Correction for Area Variation.

The second step of radiometric correction requires appropriate models to represent the terrain-dependent angular variations. In the case of microwave remote sensing applications, the theory can explain microwave scattering mechanisms from natural surfaces only to a limited extent, and the requested ground truth information such as crown height, trunk/branches dielectric constant, primary and secondary branch sizes, soil roughness or soil dielectric constant is often not available. Therefore, empirical or semi-empirical models may be preferred (Bayer *et al.*, 1991; Ruck *et al.*, 1970; Schreier, 1993).

A simple cosine backscatter model Equation (6) was used to reduce the angular variation (Ruck *et al.*, 1970) from the terrain. Equation (7) is the corresponding correction model applied to the digital numbers from an image:

$$\sigma^{\circ}_{cor} = \frac{\sigma^{\circ}}{\cos(\alpha_i)} \qquad (6)$$

$$I_{cor2} = \frac{I_{cor1}}{\sqrt{\cos(\alpha_i)}} \qquad (7)$$

where α_i is the local incidence angle, which was calculated using the equation presented by Smith *et al.* (1980):

$$\cos(\alpha_i)=\cos(\alpha_{ref})\cos(\theta_n)+\sin(\alpha_{ref})\sin(\theta_n)\cos(\phi_s - \phi_n) \qquad (8)$$

where α_{ref} is the reference incidence angle, θ_n is the local ground slope, ϕ_n is the local ground aspect, and ϕ_s is the azimuth of satellite. Figure 7 shows the result of this second step in the radiometric correction process as applied to the April image.

4) Statistical Analysis

After the georectification, digital numbers (DNs) of backscatter and coherence image data were extracted for each of the ground cover type reference locations in preparation for statistical analysis. In addition, the backscatter values were used in two very

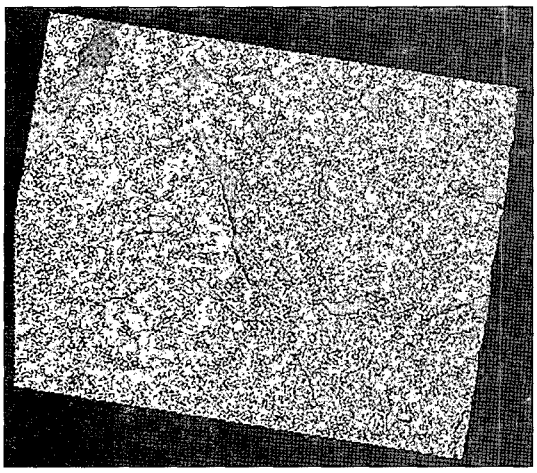

Figure 7. A Portion of the April Image after Radiometric Correction for the Area and Angular Variation.

simple approaches for investigating the multi-temporal nature of the images. The first approach studied the mean of the April and June DNs and the second approach looked at the difference in the DNs. All the extracted and computed image values were then used in a number of statistical procedures designed to indicate the separability of the three forest classes using each type of image data. Scatter plots graphically portrayed the relationships of the image values for the three classes. The mean, standard deviation, and the coefficient of variation were computed and analyzed for each class and for each type of image value. Then the Analysis of Variance (ANOVA) with a completely randomized design was applied to provide pairwise tests of the statistical differences among the three forest types for each image type (Kuehl, 1994). The null hypothesis tested in ANOVA is that all the population means are equal. Stated:

$$H_0: \mu_{sw} = \mu_{mw} = \mu_{hw}$$

where μ is the mean of each forest class type. When the null hypothesis is rejected, which means that at least one of the forest types is separable from the other types, multiple pairwise comparisons were performed using the least significant difference (LSD), Tukey's Honestly Significant Difference (HSD), and Student-Newman-Kuels (SNK) procedures (SAS Institute, 1999).

The separability among forest types was investigated using the Mahalanobis Distance Analysis using SAS. Mahalanobis distance is a useful way of determining the similarity of an unknown sample set to a known one. It is based on correlations between variables by which different patterns can be identified and analysed and takes into account the correlations of the data set (Manly, 1994). For this study, Mahalanobis distance values were calculated from the combined radar measurements of coherence with the backscatters of April and June (radiometrically corrected for area and angular variation).

3. Results

Table 1 summarizes the means, standard deviations and coefficients of variation statistics for each type of JERS-1 radar image values and for the three forest classes. Generally, this table indicates some limited capability of differentiating the forest types based on simple backscatter measurements from single images, except for the mixedwood from the hardwood. However, the table shows improved capabilities when the data were radiometrically corrected for the terrain effects, especially when the data were corrected for both the area and the angular variations. This may be due to the fact that the radiometric correction decreases the variance (standard deviation) associated with each class while maintaining or increasing the separation of the means. As would be expected, the mean backscatter statistics exhibit a pattern very similar to the backscatters of April and June. The backscatter difference statistics were

Table 1. Statistics of Forest Types for Various Radar Image Measures.

Radar Image Measure[1]		Hardwood		Mixedwood		Softwood	
		Mean	Standard Deviation	Mean	Standard Deviation	Mean	Standard Standard
Coherence[2]		77.26	14.17	99.72	21.83	126.03	25.58
No Radiometric Correction[3]	April Backscatter	1045.58	159.67	1052.79	99.49	1225.83	156.52
	June Backscatter	983.78	162.78	1053.72	101.77	1204.94	175.19
	Mean Backscatter (April, June)	1014.68	158.04	1053.26	92.00	1215.39	156.99
	Backscatter Difference (April-June)	61.80	63.91	-0.93	81.56	20.89	108.58
Radiometric Correction for Area Variation[4]	April Backscatter	1008.82	90.12	1078.49	76.19	1231.53	121.34
	June Backscatter	948.52	106.37	1079.31	76.31	1209.26	133.42
	Mean Backscatter (April, June)	978.67	93.44	1078.90	64.06	1220.39	115.64
	Backscatter Difference (April-June)	60.30	62.83	-0.82	82.72	22.28	107.55
Radiometric Correction for Area and Angular Variation[5]	April Backscatter	1130.25	82.49	1240.59	86.00	1413.02	96.19
	June Backscatter	1062.13	106.18	1241.03	79.69	1386.71	106.61
	Mean Backscatter (April, June)	1096.19	88.15	1240.81	67.99	1399.87	81.18
	Backscatter Difference (April-June)	68.12	71.26	-0.44	94.88	26.31	121.96

[1] Each sample value was calculated by averaging the image values in a 100m by 100m window.
[2] Digital number of the coherence image, calculated from equation 1, and its value (from 0 to 1) scaled from 0 to 255.
[3] Digital number of the backscatter image: No correction applied.
[4] Digital number of the backscatter image corrected for area variation, calculated from equation 5.
[5] Digital number of the backscatter image corrected for area and angular variation, calculated from equation 7.

affected very little by the radiometric processing and showed little capability of distinguishing between these classes. Notably, using uncorrected backscatters distinguished the hardwood from the softwood to a limited degree, but radar coherence appears to have some potential for distinguishing among all three classes. This potential exists even though the general coherence values are low.

Scatter plots of the data support the trends shown by the simple statistics and show some interesting results. Figures 8-a, b, and c show the advantages of applying radiometric correction for the terrain effects, especially applying the correction for both the area and the angular variations. The confusion among classes in Figure 8-b is lower than for the overlap shown in Figure 8-a (the variance of the hardwood decreases more than others), and Figure 8-c shows even lower confusion among these classes. Figure 8-d shows some ability to separate the hardwood and the softwood using only the coherence. Coherence generally increases as you consider the hardwood, then the mixedwood, and finally the softwood. However, the coherence of the mixedwood class overlays the other classes considerably. Also, Figures 8-e and 8-f show that the coherence appears to add some unique classification information, but not to a desirable extent.

Table 2 summarizes the results from the ANOVA and shows statistical significance for the separation of the class means for most image measurements. The ANOVA results again clearly show the effectiveness of radiometrical correcting for terrain and viewing-angle effects. Both types of corrected results (the correction for area variation and the correction for both the area and angular variations) show the separation of all three classes, while the uncorrected backscatters (from both dates) fail to distinguish the mixedwood from the hardwood.

These statistical results indicate that the coherence, the April backscatter (corrected for the area and

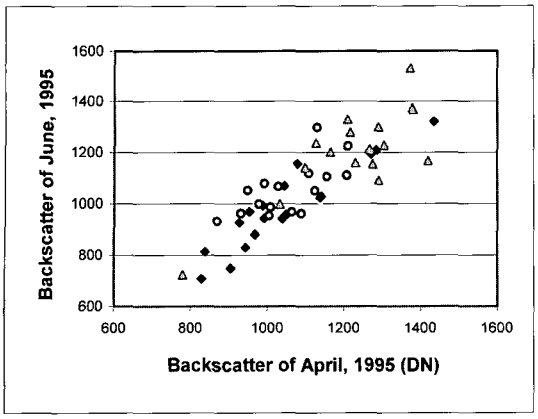

a. The Backscatter of April vs. June (uncorrected).

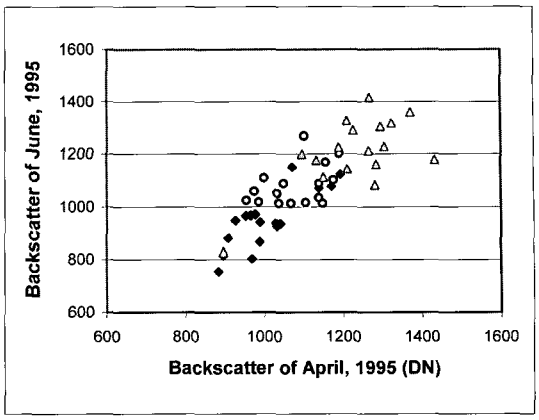

b. The Backscatter of April vs. June (corrected for area variation).

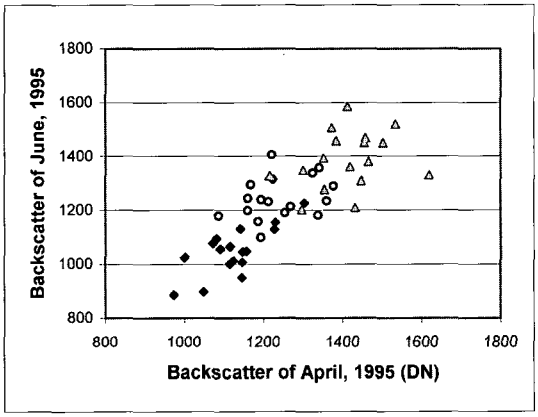

c. The Backscatter of April vs. June (corrected for area and angular variation).

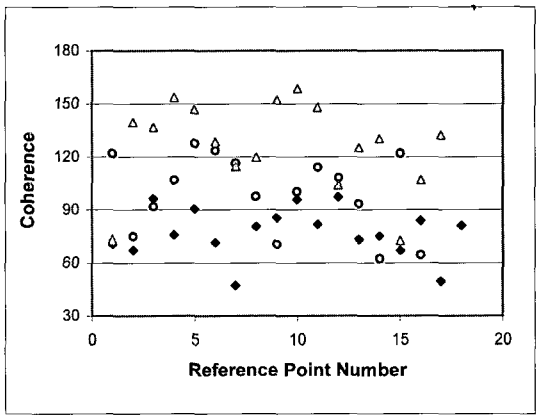

d. The Coherence.

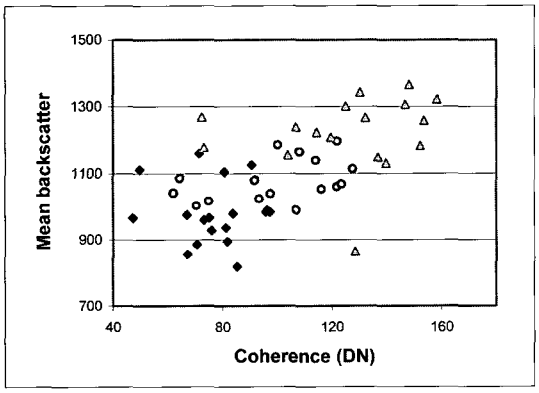

e. The Coherence vs. Mean Backscatter of April and June (Corrected for the Area Variation).

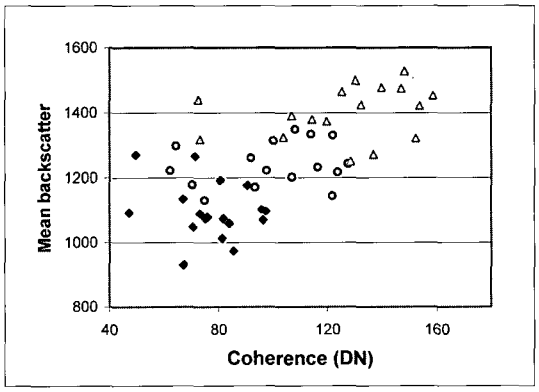

f. The Coherence vs. Mean Backscatter of April and June (Corrected for the Area and Angular Variation).

◆ Hardwood
o Mixedwood
△ Softwood

Figure 8. Scatter Plots for the Analysis of Each Data. The values for y-axis are DN.

Table 2. Summary Results of Analysis of Variance.

Radar Measurement	Overall Significance of F statistic for Forest Classes	Pairwise Comparison results of Forest Classes[1]
Coherence (April with June)	0.0001	SW from MW from HW
April Backscatter (uncorrected)	0.0006	SW from MW and HW
April Backscatter (corrected for area variation)	0.0001	SW from MW from HW
April Backscatter (corrected for area and angular variation)	0.0001	SW from MW from HW
June Backscatter (uncorrected)	0.0003	SW from MW and HW
June Backscatter (corrected for area variation)	0.0001	SW from MW from HW
June Backscatter (corrected for area and angular variation)	0.0001	SW from MW from HW

[1] Results from the least significant difference (LSD), Tukey's Honestly Significant Difference (HSD), and Student-Newman-Kuels (SNK) pairwise comparison tests (significance level 0.05) when two of the three methods gave the same conclusion.

Table 3. Mahalanobis Distance Values of the Combined Radar Measurements of the Coherence with the Backscatters of April and June (Radiometrically Corrected for the Area and Angular Variation).

Forest Classes	HW		MW		SW	
	Squared Mahalanobis Distance	Significance level	Squared Mahalanobis Distance	Significance level	Squared Mahalanobis Distance	Significance level
HW	0.0000	1.0000	4.4873	0.0001	18.2244	0.0001
MW	4.4873	0.0001	0.0000	1.0000	5.1468	0.0001
SW	18.2244	0.0001	5.1468	0.0001	0.0000	1.0000

angular variations), and the June backscatter (corrected for the area and angular variations) may together prove to be capable of separating the three forest classes. As a test, these three variables were used to compute the Mahalanobis distances between classes. The overall probability value for the multivariate analysis was less than 0.0001, which shows there is a significant difference between these three classes. Table 3 shows the Mahalanobis distances between these classes and the corresponding probability values. Apparently, the multivariate use of these three radar measurements successfully distinguished the forest types.

4. Discussion

As mentioned before, the coherence was generally very low for the heavily forested study region and the long separation of image dates (44 days). These very low values limited the effectiveness of interferometry techniques in forest classification. The low coherence also produced an interferogram insufficient to produce the phase information necessary for deriving a good quality DEM that could be used to geocode the coherence and backscatter image data.

The study area for this project can be characterized as rugged and mountainous. Due to the geometry of the side-looking sensor and the variable terrain, the backscatter of the JERS-1 SAR data exhibited a substantial radiometric variation. The backscatter of

the areas with the slope facing the sensor was greater than that of flat areas or the areas facing away. Therefore, the backscatter variations caused by the interaction of microwave energy and different forest types were masked by the differences caused by the topography. Hence, for regions with terrain variations, radar backscatters must be radiometrically corrected to account for the effect of topography. The results show that an uncorrected backscatter has a limited capability of separating the softwood from the mixedwood or the hardwood, but no capability for distinguishing the mixedwood from the hardwood. After the terrain correction, i.e., normalization for the scattering area and correction for the angular variation using a simple backscatter correction model, the results showed substantially better capabilities for classifying the forest groupings. Even the single-date and single-band backscatter data appeared to be capable of distinguishing the three types. Apparently, the L-band microwave energy interacts with the primary and secondary branches and trunks of the trees, including some interactions with the ground and trunk-ground double bounce. Tree and stand structures differ between the hardwood and the softwood. For the hardwood, the interaction with primary branches seems to dominate, while for the softwood, interaction with trunk and trunk-ground double bounce was important. Therefore, the backscatter from the softwood is greater than that from the mixedwood, and the mixedwood backscatter is greater than that from the hardwood.

The multi-temporal analysis of the backscatter was inconclusive since the backscatter within each of the three forest classes did not vary greatly between the two dates. This lack of change indicates that the presence of leaves on hardwood type trees do not contribute greatly to the magnitude of the signal return. This study verified that at the L-band wavelengths, leaves are not the primary scatterers of a forest canopy. However, the backscatter of the hardwood in the leaf-off condition is a little higher than that in the leaf-on condition. This trend indicates that the leaves act as attenuators in the L-band wavelengths.

The coherence produced from an interferometric pair of images also showed a potential for mapping forest subclasses. The coherence for the softwood stands was higher than that for the mixedwood stands and the coherence for the mixedwood stands was higher than that for the hardwood stands. This is evident even though the coherence of all forest types was quite low. This trend is also consistent with the idea that the softwood would remain fairly constant between the two dates, leading to relatively high coherence. The mixedwood would show substantial changes between the dates (and therefore lower the coherence) because the deciduous component would show lower coherence while the softwood component would remain relatively consistent. The hardwood stands would show the lowest coherence between the two dates. This trend may indicate that the emergence of leaves affects the phase information, causing some decorrelation and therefore affecting the coherence. Although this trend seems to indicate a temporal basis, a more probable reason is spatial. The hardwood and the softwood have different structures, and coherence is computed using local regions for each pixel. This process might be sensitive to the spatial relations between the softwood and hardwood species that intermingle in a mixedwood forest. The emergence of the coherence trend in this study is especially encouraging given the separation in time of the two images and the low coherence shown in the overall images. In particular, the environmental moisture, temperature and other weather conditions might contribute substantially to the lack of coherence. Therefore, real-time interferometry or short separation time repeat-pass interferometry may give higher overall

coherence and be more useful for discriminating forest types.

For a variety of reasons, repeat-pass interferometry to generate a DEM was not possible for the heavily forested region used in this study. The overall coherence in the images was so low that a sufficient interferogram could not be generated to produce a DEM. Therefore, an external DEM was registered to simulate a slant range DEM. The simulated information was then used in the interferometry process to georectify the coherence and backscatter images. There is a theoretical foundation for the simulation process, but the external DEM is reliable and sufficient ground control should be acquired. Both of these requirements might be suspect in a heavily forested and remote region like this study area.

Although multi-temporal analysis of backscatter was inclusive, it was found that there was also a potential in combining the backscatter images from the two dates with the coherence in a multivariate approach to classification. It is very likely that even better results would have been obtained if there had been multi-polarization and multi-band information. For example, JERS-1 L-band backscatter and coherence data could be fused with C-band backscatter and coherence data from the ERS or Radarsat satellites, or with longer microwave wavelengths (e.g., P-band). HH polarization data could also be fused with the HV or VH polarization data. This type of multivariate approach is also likely to be effective if SAR data are fused with other channels of remote sensing data, such as optical or thermal channels. More research on SAR application needs to be done in the future.

5. Conclusions

This study reports the results of a statistical analysis about the capability of JERS-1 L-band backscatter and coherence data to discriminate a part of Northeastern U. S. forests into softwood, mixedwood, and hardwood types. Based on numerous samples, it was found that the JERS-1 SAR data have a potential to distinguish these classes. Implementing a radiometric correction for the terrain effects substantially improved the results. The coherence produced from a repeat-pass interferometric pair of images enhanced the ability to classify forest types. However, using repeat-pass interferometry of JERS-1 imagery for producing DEMs in the study area of this research appears to be impractical because of the very low overall coherence. The heavily forested conditions and long time separation of the images prevent the ability to produce an interferogram sufficient for producing a DEM. This project applied a method to produce a georectified coherence image using a reliable external DEM. Efforts should be made in the future to analyze the JERS-1 data in conjunction with using backscatter and coherence data from different radar bands or different polarization characteristics. Fusion of the L-band and the optical data also holds promise for more reliable forest characterization from satellite platforms. SAR is a promising data provider for better imagery classification, especially, in the northeastern U. S. A., where frequent cloud contamination exists.

Acknowledgment

We thank late Paul F. Hopkins and late William Johnson for their guidance and helpful suggestions. We also thank the staff of the Mapping Science Lab

of the College of Environmental Science and Forestry, the State University of New York for their administrative and materialstic support for this research.

References

Angelis, C. F., C. C. Freitas, D. M. Valetriano, and L. V. Dutra, 2002. Multitemporal analysis of land use/land cover JERS-1 backscatter in the Brazilian tropical rainforest. *Interntion Journal of Remote Sensing*, 23(7): 1231-1240.

Askne, J. I. H., P. B. G. Dammert, L. M. H. Ulander, and G. Smith, 1997. C-band repeat-pass interferometric SAR observations of the Forest. *IEEE Transactions on Geoscience and Remote Sensing*, 35(1): 25-35.

Atlantis Scientific Inc., 1999a. *EarthView APP User's Guide*, Version 1.5, Nepean, Ontario, Canada, 149p.

Atlantis Scientific Inc., 1999b. *EVInSAR User's Guide*, Version 1.2, Nepean, Ontario, Canada, 318p.

Bayer, T., R. Winter, and G. Schreier, 1991. Terrain influences in SAR backscatter and attempts to their correction. *IEEE Transactions on Geoscience and Remote Sensing*, 29(3): 451-462.

Beaudoin, A., N. Stussi, D. Troufleau, N. Desbois, L. Piet, and M. Deshayes, 1995. On the use of ERS-1 SAR data over hilly terrain: necessity of radiometric corrections for thematic applications. *Proceedings of International Geoscience and Remote Sensing Symposium*, Vol. 3, 10-14 July 1995, Firenze, Italy, pp. 2179-2182.

Curlander J. and R. McDonough, 1991. *Synthetic Aperture Radar: Systems and Signal Processing*, John Wiley and Sons, Inc., New York, 647p.

Elachi C., 1998. *Spaceborne Radar Remote Sensing: Applications and Techniques*, IEEE Press, New York, 255p.

European Forests Observation by Radars (EUFORA), 1998, URL: http://www.rss.chalmers.se/WWW_rsg/Research/Projects/EUFORA/EUFORA_FinalReport.pdf.

Gens, R. and J. L. Van Genderen, 1996. SAR interferometry-Issues, techniques, applications. *International Journal of Remote Sensing*, 17: 1803-1835.

Henderson, F. M. and A. J. Lewis, 1998. *Principles and Applications of Imaging Radar, Manual of Remote Sensing*, Third Edition, Vol. 2, John Wiley & Sons, Inc., New York, 866p.

Huurneman, G., R. Gens and L. Broekema, 1996. Thematic information extraction in a neural network classification of multi-sensor data including microwave phase information. *International Archives of Photogrammetry and Remote sensing*, Vol. XXXI, Part B2, pp. 170-175.

Johnson, Richard. A. and D. W. Wichern, 1998. Applied Multivariate Statistical Analysis. 4th Ed. Prentice Hall.

Kinn, Gerald, 2002. Direct Georeferencing In Digital Imaging Practice. *Photogrammetric Engineering and Remote Sensing*, 68(5): 399-402.

Kuehl, Robert, 1994. Design of Experiments: Statistical Principles of Research Design and Analysis. 2nd ed. Duxbury Press.

Manly, Bryan. F. J., 1994. Multivariate Statistical Methods: A Primer, 2nd Ed. Chapman & Hall/CRC.

Raney, R. K., T. Freeman, R. W. Hawhins, and R. Bamler, 1994. A plea for radar brightness.

Proceedings of International Geoscience and Remote Sensing Symposium, Vol. 2, 8-12 Aug. 1994, Pasadena, CA, U.S.A., pp.1090-1092.

Rignot, E. J. M., C. L. Williams, J. Way, and L. A. Viereck, 1994. Mapping of Forest Types in Alaskan Boreal Forests Using SAR Imagery. *IEEE Transactions on Geoscience and Remote Sensing*, 32(5): 1051-1059.

Rodes, E. and S. Saatchi, 2002. Application of multiscale texture in classifying JERS-1 radar data over tropical vegetation. *Interntion Journal of Remote Sensing*, 23(7): 1487-1506.

Ruck, G. T., D. E. Barrick, W. D. Stuart, and C. K. Krichbaum, 1970. *Radar Cross Section Handbook*, Editor: George T. Ruck, Volume 2, Plenum Press, New York-London, 949p.

Salas, W. A., M. J. Ducey, E. Rignot, and D. Skole, 2002a. Assessment of JERS-1 SAR for monitoring secondary vegetation in Amazonia: I. Spatial and temporal variability in backscatter across a chrono-sequence of secondary vegetation stands in Rondonia. *Interntion Journal of Remote Sensing*, 23(7): 1357-1379.

Salas, W. A., M. J. Ducey, E. Rignot, and D. Skole, 2002b. Assessment of JERS-1 SAR for monitoring secondary vegetation in Amazonia: II. Spatial, temporal, and radiometric considerations for operational monitoring. *Interntion Journal of Remote Sensing*, 23(7): 1381-1399.

SAS Institute, 1999. SAS/STAT User's Guide, Version 8, STATS Publishing Inc.

Schreier, G., 1993. *SAR Geocoding: Data and Systems*, Chapter 14, Karlsruhe: Wichmann, 435p.

Sgrenzaroli, M., G. F. De Grandi, H. Eva, and F. Achard, 2002. Tropical forest cover monitoring: estimates from the GRFM JERS-1 radar mosaics using wavelet zooming techniques and validataion. 23(7): 1329-1355.

Shimada, M. and Isoguchi, O., 2002. JERS-1 SAR mosaic of Southeast Asia using calibrated path images. *Interntion Journal of Remote Sensing*, 23(7):1507-1526.

Shimada, M., 1996. Radiometric and Geometric calibration of JERS-1 SAR. *Advances in space research*, 17(1): 79-88.

Simard, M. G. D. Grandi, S. Saatchi, and P. Mayaux, 2002. Mapping tropical coastal vegetation using JERS-1 and ERS-1 radar data with a decision tree classifier. *Interntion Journal of Remote Sensing*, 23(7): 1461-1474.

Smith, J. A., 1980. The Lambertian assumption and Landsat data. *Photogrammetric Engineering and Remote Sensing*, 46(9): 1183-1189.

Stofan, E. R., D. L. Evans, C. Schmullius, B. Holt, J. J. Plaut, J. van Zyl, S. D. Wall, and J. Way, 1995. Overview of results of spaceborne imaging radar-C, X-band synthetic aperture radar (SIR-C/X-SAR). *IEEE Transactions on Geoscience and Remote Sensing*, 33(4): 817-828.

Strozzi, T., P. B. G. Dammert, U. Wegmuller, J. M. Marinex, J. I. H. Askne, A. Beaudoin, and M. T. Hallikainen, 2000. Landuse mapping with ERS SAR interferometry. *IEEE Transcations on Geoscience and Remote Sensing*, 38(2): 766-744.

Torma, M. and J. Koskinen, 1997. Land-use classification using temporal SAR-images, *Proceedings of International Geoscience and Remote Sensing Symposium*, Vol. 1, Singapore, pp. 44-46.

Ulaby, F. T., R. K. Moore, A. K. Fung, 1982. *Microwave Remote Sensing: Active and Passive*, Chapter 7, Vol.2, Addison-Wesley Publishing Company: Massachusetts, 2162p.

Ulander, L. M. H., 1996. Radiometric slope correction of synthetic-aperture radar images. *IEEE Transactions on Geoscience and Remote Sensing*, 34(5): 1115-1122.

U.S. Geological Survey, 1998. URL: http://www.apa.state.ny.us/gis/shared/htmlpages/metadata/10mDEM.html

Van Zyl, J. J., B. D. Chapman, P. Dubois, and J. Shi, 1993. The effect of topography on SAR calibration. *IEEE Transactions on Geoscience and Remote Sensing*, 30(5): 1036-1043.

Wegmuller, U. and C. L. Werner, 1995. SAR interferometric signatures of forest. *IEEE Transactions on Geoscience and Remote Sensing*, 33(5): 950-959.

Wegmuller, U. and C. L. Werner, 1997. Retrieval of vegetation parameters with SAR interferometry. *IEEE Transactions on Geoscience and Remote Sensing*, 35(1): 18-24.

Wegmuller, U., T. Strozzi, and C. Werner, 1997. Forest applications of ERS, JERS, and SIR-C SAR interferometry. *Proceedings of International Geoscience and Remote Sensing Symposium*, Vol. 2, Singapore, pp. 790-792.